Colloids and Surfaces B: Biointerfaces 217 (2022) 112709

Contents lists available at ScienceDirect

Colloids and Surfaces B: Biointerfaces

journal homepage: www.elsevier.com/locate/colsurfb

Initial bacterial retention on polydimethylsiloxane of various stiffnesses: The relevance of modulus (mis)match

Viktoriia Drebezghova [c], Florence Hakil [c], Régis Grimaud [c], Hubert Gojzewski [a], G. Julius Vancso [b], Corinne Nardin [c,*]

[a] Sustainable Polymer Chemistry, Faculty of Science and Technology, University of Twente, 7500AE Enschede, the Netherlands
[b] Materials Science and Technology of Polymers, and Sustainable Polymer Chemistry, Faculty of Science and Technology, University of Twente, 7500AE Enschede, the Netherlands
[c] Université de Pau et des Pays de l'Adour, E2S UPPA, CNRS, IPREM, 64000 Pau, France

ARTICLE INFO

Keywords:
Bacterial retention
PDMS
Mechanical stiffness
Atomic force microscopy
Surface modulus

ABSTRACT

Initial retention of the bacterium *Escherichia coli* on model poly(dimethylsiloxane) (PDMS) surfaces was studied as a function of substrate bulk and surface mechanical stiffness values. Our reference PDMS system was designed such that out of the parameters that govern bacterial adhesion only the mechanical stiffness was systematically varied. This was achieved by varying the crosslinking density of PDMS. Following crosslinking, we performed Soxhlet extraction of non-crosslinked, free chains to rule out their effect on bacterial response. Bulk moduli were assessed by dynamic mechanical analysis at 1 rad sec^{-1} frequency and the values obtained ranged between 0.03 and 1.8 MPa. The increase in crosslink density resulted in increasing surface modulus, as measured by atomic force microscopy, with values ranging between 0.7 and 9 MPa. The number of bacteria retained was then assessed. We observed a decreasing trend with the increase of both bulk and surface mechanical stiffnesses down to a limit corresponding to the Young's modulus of the bacterial cell surface. For higher values than this threshold, the number of retained bacteria remained constant. We tentatively explain this observation by considering conformal overlay of bacterial and material surfaces.

1. Introduction

Controlling the colonization of materials by microorganisms is crucial in a wide range of industrial and clinical settings. Biofilms include surface associated bacterial communities embedded in a hydrogel-like matrix, in which high cell density, reduced diffusion and physicochemical heterogeneity play a role and induce adaptive cell behaviors. However, the underlying mechanisms that govern the interactions of bacteria with surfaces remain poorly understood, limiting the ab initio design and engineering of biomaterials to control bacterial attachment and further biofilm growth [1]. Preventing biofilm formation thus necessitates enhanced understanding to hinder the initial stage of bacterial adhesion.

The materials properties, often intricately entangled, which alter bacterial attachment include chemistry, hydration, surface charges, the topography, and mechanical properties [2]. Owing to continuous advances in polymer chemistry, polymer-based devices have become increasingly used to reduce chronic infection and medical device failure [3,4]. Various antimicrobial polymers, polymer-based hydrogels and polymer coated surfaces are being developed for various applications such as wound healing [5], stem cell encapsulation [6] and bone tissue engineering [7]. However, to date, the research conducted in the field of antimicrobial polymers has focused mostly on their chemical and structural aspects [8–11] and the outcomes evidence the difficulty to disentangle the role of surface chemistry, hydration state and electric charge from the intrinsic material mechanical properties.

As examples for the complex interplay, poly(ethylene glycol) (PEG) hydrogels of various thicknesses, resistant to protein adsorption, were immobilized on glass slides [12]. Results show, that the thinner the hydrogel the higher the number of adherent bacteria. The underlying stiff substrate may however also influence the perceived mechanical properties of the hydrogel by the adherent bacteria. As another example, it was shown, using both PEG hydrogels and hydrated brushes, that the mechanical properties, the molecular architectures and the thicknesses of PEG-based coatings all influence the flow-driven surface motion of *Staphylococcus aureus* MS2 cells [13]. These investigations further

* Corresponding author.
E-mail addresses: g.j.vancso@utwente.nl (G.J. Vancso), corinne.nardin@univ-pau.fr (C. Nardin).

https://doi.org/10.1016/j.colsurfb.2022.112709
Received 21 February 2022; Received in revised form 23 June 2022; Accepted 17 July 2022
Available online 19 July 2022

highlight the difficulty to assess which one of the parameters, the moduli and/or the local polymer concentration plays a critical role.

To rule out the role of hydration and surface charges on bacterial adhesion, elastomers, which are solvent-free, are of particular interest, especially poly(dimethylsiloxane) (PDMS), which is a polymer used in various biomedical applications. The first systematic study on the effect of the stiffness of PDMS on bacterial adhesion was conducted by Song et al. [14,15]. The authors reported that the stiffness of PDMS of Young's moduli ranging between 0.1 and 2.6 MPa does not only affect the attachment of bacteria but also the morphology and the antibiotic susceptibility of the attached cells [14,15]. They suggested that the degree of deformation of the bacterial cell membrane upon contact with the PDMS surfaces of differing stiffness does affect bacterial mechanosensing. This conclusion was based on the observation that the level of the intracellular second messenger, cyclic diguanylate monophosphate, decreased with PDMS stiffness [16].

Allain and coworkers systematically tuned the substrate topography and stiffness of PDMS substrates while keeping the surface free energy constant [17]. The authors used low energy singly charged inert ions to irradiate PDMS to achieve substrates of variable stiffness, but exhibiting comparable surface free energy. However, this process resulted in the formation of a wavy (wrinkled) topography at the PDMS surface, which could also affect bacterial surface attachment even in very compliant PDMS (Young's moduli of 0.02 and 0.2 MPa).

In another study, [18] using polystyrene beads (PS), the authors showed that bacterial adhesion on PDMS samples of Young's moduli ranging from 0.06 to 4.52 MPa is a physical process, which is not mediated by bacterial surface appendages. In a subsequent approach, PDMS surfaces of differing stiffnesses coated with a 2 nm highly crosslinked hexamethyldisiloxane (HDMSO) were used to confer comparable surface chemistry, while retaining similar mechanical properties for coated and uncoated samples [19]. The authors came to the conclusion that uncoated PDMS of low Young's modulus contained free polymer chains and longer chain ends at the surface, which lead to higher bacterial adhesion.

In order to shed further light on the complex issue of cell-substrate adhesion and the impact on it by surface elasticity, we performed systematic research described here. To exclude the role of free chain PDMS, we resorted to their Soxhlet extraction. We varied the surface stiffness of PDMS and monitored initial retention while keeping the other surface characteristics unaltered. We investigated initial bacterial retention, which is essential since at the very early stage of surface colonization, solely strongly adhered bacteria would eventually enable further biofilm growth [20]. Bulk and advanced surface characterization techniques, in particular atomic force microscopy (AFM) and X-ray photoelectron spectroscopy (XPS) were used to show that the material surface chemistry and topography do not depend on the degree of crosslinking of the elastomer.

2. Material and methods

2.1. Materials

Cyclohexane ($\geq$ 99%, GPR RECTAPUR®) and acetone ($\geq$ 99%) were supplied by VWR Chemicals (Fontenay-sous-Bois, France). Phosphate buffered saline (PBS) (137 mM NaCl, 2,7 mM KCl, 10 mM Na_2HPO_4, 1,76 mM KH_2PO_4, pH = 4.4), chloramphenicol ($\geq$ 98%) and the nonionic detergent Tween20 were purchased from Sigma-Aldrich (St-Quentin-Fallavier, France). Lysogeny broth (LB) and LB agar (for the preparation of plates) were purchased from Difco (Saint-Ferréol, France).

2.2. Bacterial strain and growth medium

The model *E. coli* strain used was DH5α carrying the plasmid pSEVA337 which contains the green fluorescent protein (GFP) gene under the control of the constitutive Pem7 promoter [21]. pSEVA337 carrying the resistance to chloramphenicol was obtained from the Standard European Vector Architecture 3.0. The strain was routinely grown at 37 °C in LB and LB agar supplemented with 34 μg mL^{-1} chloramphenicol (to maintain the plasmid).

2.3. Preparation of PDMS surfaces

PDMS samples were prepared using the Sylgard-184 silicone elastomer kits purchased from the Dow Chemical Company (supplied by Samaro, Lyon, France). The stiffness was adjusted by varying the crosslinker concentration (curing agent to base ratio expressed in weight percent) and thus the crosslinking density. For each crosslinker concentration (2.5, 5, 10, 20, and 25 wt%), the elastomer base and curing agent were thoroughly mixed and degassed under vacuum for 30 min. Then, the mixture was poured into a Petri dish, cured at 60 °C for 24 h, and subsequently incubated at room temperature for another 24 h to achieve complete cross-linking. After curing, the PDMS samples (1 mm thick) were removed from the Petri dish and specimens were punched out with diameters according to the need. The samples were then cleaned by soaking in 70% ethanol for 20 min, prior to a rinsing step in Milli-Q water.

To extract not crosslinked, free chains, samples prepared at various cross-linker concentrations (2.5, 5, 10, 20, and 25 wt%) were subjected to Soxhlet extraction in acetone/cyclohexane (1:1 mixing ratio) for 48 h at 6 cycles per hour (over 250 wash cycles). Specimens were then dried in vacuum at 80 °C for 24 h. The mass of each PDMS sample was measured before the extraction and subsequent to the drying step. The softest specimen at 2.5 wt% of cross-linker could not be recovered subsequent to extraction.

2.4. Methods

2.4.1. Thermogravimetric analyses (TGA)

Thermogravimetric (TGA) analyses was performed with the uncrosslinked material, i.e., on each component (base and crosslinker) separately, as well as on the crosslinked PDMS specimen at 20 wt% of cross-linker. The TGA curves were obtained on a thermogravimetric analyzer Q50 (TA Instruments, New Castle, DE, USA). The experiments were carried out under a nitrogen flow, at a heating rate of 20 °C min^{-1}, at temperatures ranging from 40° to 1000°C.

2.4.2. Fourier transform infrared (FTIR) spectroscopy

FTIR spectroscopy was performed on both the pre-polymer (base) and the cross-linker components, as well as on cured PDMS samples at different cross-linker concentrations (2.5, 5, 20, and 25 wt%). The FTIR spectra were measured using a Perkin-Elmer Spectrum One FTIR Spectrometer (Waltham, Massachusetts, USA). The spectra of the pre-polymer and cross-linker were captured in the transmission mode between 650 and 4000 cm^{-1}, at a 4 cm^{-1} resolution. To this end, a thin layer of each PDMS component (~ 100 μm) was spread between two polyethylene films (10 μm in thickness) and then mounted into the sample chamber prior to measurements. The background spectrum of the clean polyethylene films was subtracted from those of the recorded FTIR spectra. The cross-linked PDMS samples were measured in the attenuated total reflection (ATR) mode in the same spectral range.

2.4.3. Dynamic mechanical analysis (DMA)

The dynamic mechanical properties of bulk PDMS before and after extraction were evaluated by measuring the storage modulus (real part of the complex shear modulus, G) in the parallel-plate geometry. The experiments were carried out with both pristine and extracted PDMS specimens at various cross-linker concentrations (2.5, 5, 10, 20, and 25 wt%), cylindrical in shape (Ø 8 mm, 1 mm thickness) at 25 °C.

First a stress sweep test was performed between 10 and 1000 Pa at a constant frequency of 2 rad·s^{-1} and at 25 °C. The storage (G′) and loss

(G') moduli were found to be independent of the applied shear stress. Frequency sweep tests were done in the range from 80 to 0.045 rad·s^{-1} at the applied shear stress of 50 Pa and at 25 °C. All measurements were performed at 10 N applied normal force to avoid slip at the interface between the plates and the specimens. Experiments were repeated three times.

A control test in "no-slip" condition was also performed on a series of PDMS samples (2.5, 5, 10, 20, and 25 wt% cross-linker concentration), cured within the rheometer (in situ) to provide a firm adhesion between the specimen and the plates. We performed these experiments to ensure that slip did not take place. The in situ cured control specimens of 8 mm in diameter and 1 mm in thickness were characterized using the same measurement conditions. The applied normal force was fixed at 0.5 N during the frequency sweep measurements.

The bulk Young's moduli of the cross-linked PDMS were calculated from storage modulus measurements using the relation between the Young's modulus, E, and the shear storage modulus $E = 2G'(1+\nu)$, where ν is Poisson's ratio. A value of ν of 0.5 for PDMS was taken from the literature [22].

2.4.4. Contact angle measurements

The wetting properties of pristine and extracted PDMS surfaces were measured via the static contact angle method using a custom made optical tensiometer. The water droplet volume was of 6–7 μL. A total of 10 droplets were analyzed using the ImageJ software. All contact angle measurements were conducted at room temperature (21 °C).

For the surface free energy determination, contact angle data of two additional probe liquids, hexadecane and diiodomethane, were measured and analyzed for each sample following the same procedure as with the water droplets. The surface free energy was then determined using the Owens-Wendt equation [23].

2.4.5. X-ray photoelectron spectroscopy (XPS)

XPS spectra were collected on a Quantera SXM (scanning XPS microprobe) from Physical Electronics (aluminum K_α, monochromatic radiation at 1486.6 eV; base pressure $< 3 \times 10^{-8}$ Torr; detector input angle of 45°) (Feldkirchen, Germany). Compass software for XPS control and Multipak v.9.8.0.19 for data reduction were used. The fitting of the spectra was performed after shifting of the measured spectra with respect to known reference binding energies (aliphatic carbon C1s at 284.8 eV or gold Au4f7/2 at 83.96 eV, silver Ag3d5/2 at 368.21 eV and copper Cu2p3/2 at 932.62 eV).

Five spots (200 μm spot size) for each sample were analyzed, i.e., one for a survey XPS spectra and four for element spectra and their averaging. Survey XPS spectra were obtained in three cycles with the pass energy of 224 eV.

2.4.6. Atomic Force Microscopy

Pristine and extracted PDMS samples were imaged by AFM using a MultiMode 8 AFM with a NanoScope V controller (Bruker, Santa Barbara, USA), in air and at room temperature (~ 21 °C). The instrument was operated in the Peak Force Quantitative Nanomechanical Mapping mode (PF-QNM) to record force-distance curves, and further processed with the NanoScope Analysis software (version 1.9). An "E" vertical-engagement piezo-scanner was used to acquire data with high resolution. The AFM data was collected following a sine-wave sample-tip trajectory with a frequency of 2 kHz and utilizing a peak-force amplitude value of 150 nm. The ScanAsyst controlled parameters (feedback loop, applied load, etc.) in the user interface of the NanoScope software (version 9.7) were set to "off", in order to apply specific scanning settings, particularly low applied normal forces (300 pN – 1 nN) and high feedback loop gain (30 – 70). Cantilevers were used with a nominal spring constant of 0.5 N·m^{-1} and silicon-made tips had a nominal radius of 8 nm (MikroMasch, HQ:NSC19/No Al). The AFM optical sensitivity (deflection sensitivity) was calculated based on the thermal tune method [24].

The surface Young's modulus obtained by AFM was calculated by fitting the slope of the extended part of force-distance curves with a contact mechanics model based on the Derjaguin, Muller, and Toporov (DMT) theory [25] with a Poisson's ratio value of 0.5 [22].

2.4.7. Epifluorescence microscopy

Samples were mounted between a glass slide and a coverslip, and observed using an Axio Observer Z1 inverted fluorescence microscope (Zeiss, Jena, Germany) equipped with an oil immersion objective 63x NA 1.4. Green fluorescent protein-expressing cells were visualized using a BP 470/40 excitation filter, a FT 495 beam splitter, and a BP 525/50 emission filter. Images were acquired using a Zeiss Axiocam 506 mono camera monitored by the Zeiss Zen 2012 software.

2.4.8. Bacterial retention on PDMS

DH5α pSEVA337 cells, expressing the GFP, were grown in LB medium under shaking at 37 °C up to the exponential phase of growth at an optical density at 600 nm of 0.6. Cells were harvested by centrifugation at 5000 rpm for 10 min and re-suspended in PBS at an optical density at 600 nm of 0.1 corresponding approximately to 10^7 cells mL^{-1}. This bacterial suspension (≈ 30 mL) was poured in a Petri dish containing clean PDMS samples. After incubation at 37 °C for 1 h without shaking, the PDMS samples were gently washed by dipping in fresh PBS three times. Then, the adhered cells were detached from the PDMS surfaces by shaking in 10 mL of PBS containing 0.01 vol% of the Tween20 surfactant. To enumerate colony forming units (CFU) re-suspended in the surfactant-containing PBS we used the counting plate method [26]. Briefly, this procedure consists in spreading 100 μL aliquots from a series of decimal dilutions of the surfactant-containing bacterial suspension on agar plates. The plates are then incubated at 37 °C overnight to count colonies.

To check that the Tween20 did not lyse the cells during the assay, the growth of the strain in LB containing 34 μg mL^{-1} of chloramphenicol and LB containing 34 μg mL^{-1} of chloramphenicol and 0,01% Tween20 was monitored by measuring the optical density at 600 nm (see Electronic supplementary information ESI, Fig. S1).

The efficiency of bacterial detachment from PDMS surfaces rinsed in PBS containing the detergent was also probed by fluorescence microscopy (ESI, Fig. S2). To do so, two PDMS samples at 20 wt% of cross-linker were incubated in the bacterial suspension at 37 °C for 2 h. One of the samples was gently washed in three PBS rinsing baths, then a PBS droplet was deposited on the sample and a coverslip was placed on top to immobilize the cells prior to epifluorescence imaging. The second sample also treated through three PBS rinsing baths, followed by shaking in PBS with 0.01 vol% of the detergent for 20 s, was subsequently imaged by epifluorescence microscopy.

2.4.9. Statistics

The measurements of water contact angle, XPS spectra, bulk and surface Young's moduli, and network mesh size were analyzed with unpaired, two-tailed Student's *t*-test with a 0.05 level of significance. The Pearson correlation test was used to determine whether there is a significant correlation between the number of CFU and both bulk and AFM Young's modulus at 0.05 level of significance.

3. Results and discussion

For sample preparation, the Sylgard-184 silicone kit was chosen owing to its widespread use for microfluidics and biomedical applications. We produced samples of differing stiffness by varying the cross-linker concentration (2.5, 5, 10, 20, and 25 wt%) according to conventional methods (see Materials and Methods). To exclude the role of free PDMS chains on initial bacterial retention, we performed bacterial retention assays on PDMS surfaces at different cross-linking concentrations prior to, and following the removal of free PDMS chains using Soxhlet's extraction. Removal of not cross-linked, free chains by Soxhlet

extraction was first assessed by mass loss (ESI, Table S1). The mass of the extracted residue was 5 wt% of the total mass of the cross-linked specimens at 10, 20, and 25 wt% of cross-linker and 10 wt% of the total mass at 5 wt% of cross-linker. The softest specimen at 2.5 wt% of cross-linker was destroyed and could not be recovered subsequent to Soxhlet extraction, most likely due to critically low content of elastic network chains.

We first performed TGA analyses of each component (base and cross-linker) since the silica fillers used to reinforce the cross-linked elastomer matrix might alter the physicochemical properties of the material. The filler content of each component is reported in the ESI (Fig. S3). According to TGA, the pre-polymer contains about 23 wt% of remaining residue, whereas the cross-linker residue at 900 °C approaches 5 wt% although the supplier claims that the pre-polymer (base) and cross-linker contain 30–60 wt% and 10–30 wt% of silica filler, respectively [27,28]. The cross-linked PDMS sample contains 54% of residue that is considerably higher than the residue found in the pre-polymer. Delebecq et al. [29] performed a very detailed TGA study of silica-filled PDMS blends and showed that the platinum catalyst can increase the extra residue up to 40% for vinyl-functionalized silica. In the presence of platinum, PDMS chains generate cross-link points with the silica surface forming a layer of immobilized PDMS chains at the interface. Such immobilization leads to the ceramization of the chain fragments during degradation at high temperatures, and consequently to a final additional residue. From these TGA analyses we can thus conclude that the components contain far fewer silica fillers than indicated by the supplier.

Contact angle measurements with solvents of different surface tensions were further performed to determine the surface energy and revealed no significant difference prior and subsequent to Soxhlet extraction (Fig. 1 and Table S2). The water contact angle value slightly increases with increasing crosslinker concentration between (88 ± 3) ° and (104 ± 1) ° (Student's *t*-test between each pair of data, $p < 0.05$). By contrast, there is no statistically significant difference between the surface energy values of the PDMS specimens of various crosslinking density neither prior to, nor following Soxhlet extraction, except for the softest 2.5 wt% PDMS specimen.

For chemical characterization of the PDMS substrates, we carried out FTIR spectroscopy on each component (base and cross-linker). Fig. S4 (ESI) provides the absorption spectra of each component measured in the transmission mode. The two Sylgard components exhibit several common IR bands. Among the most intense are those originating from asymmetrical CH_3 stretching in $\equiv$Si–CH_3 (2960 cm^{-1}), symmetrical CH_3 stretching in $\equiv$Si–CH_3 (1410 cm^{-1}), symmetrical CH_3 deformation in $\equiv$Si–CH_3 (1260 cm^{-1}), asymmetrical Si-O-Si stretching (≈1020–1090 cm^{-1}). A broad absorption band at ≈ 790 – 850 cm^{-1} is common to both components. Aside from the similarities, the spectrum of the Sylgard cross-linker exhibits a peak at 2160 cm^{-1} assigned to the Si-H bond and the small peak at 910 cm^{-1} associated with the vinyl functional group C=CH_2. The Si-H and vinyl absorption peaks confirm the presence of the reactive functions in the cross-linker. All absorption bands are listed in ESI (Table S3).

FTIR spectroscopy was also performed on both pristine and extracted cross-linked PDMS at differing cross-linker concentrations (2.5, 5, 20, and 25 wt%) in the ATR mode. The spectra are remarkably similar (Fig. S5), except a minute increase of the low intensity peak at 910 cm^{-1} with increasing cross-linker concentration. This peak, as mentioned, arises from the vinyl functional group C=CH_2. As expected, the absorption band at 2160 cm^{-1} associated with the Si-H cross-linking agent completely vanished.

In a second stage, the elemental composition of the surface was characterized by XPS analysis prior and subsequent to Soxhlet extraction (Fig. 2). The spectra are provided in ESI (Fig. S6 to S8 for the crosslink densities 5, 10 and 20 wt% respectively) whereas Fig. 2 and Table S4 (ESI) give the elemental composition.

As can be observed in Fig. 2 and in Table S4, the elemental analysis shows that, within the experimental error, there is no statistically significant difference in the composition of the PDMS specimens as a function of the crosslinker concentration neither prior to, nor following Soxhlet extraction. Subsequent to Soxhlet extraction, the C content increases slightly whereas the O and Si content decreases at all crosslinker concentration (Student's *t*-test for each pair of data, $p < 0.05$), which can be explained not only by the removal of free, non-crosslinked PDMS chains but also of some of the silica fillers. This hypothesis is strengthened by the fact that the C content subsequent to Soxhlet extraction is higher at the lower crosslinker concentration, at which lower number of cross-link points between the silica fillers surface and the PDMS chains are generated (as monitored by TGA analysis). Overall, the elemental composition prior and subsequent to extraction is in line with the slight decrease of the surface energy monitored by static contact angle measurements.

Bulk Young's moduli values of PDMS samples were estimated using the theoretical relation (applicable to ideal cases) between the Young's modulus and the shear storage modulus, i.e. $E = 3G'$. Fig. 3 shows the Young's modulus evolution versus cross-linking concentration of both extracted and un-extracted PDMS samples. When increasing the cross-linker concentration to 10 wt%, the Young's modulus of the PDMS samples drastically increases (Student's *t*-test between each pair of data,

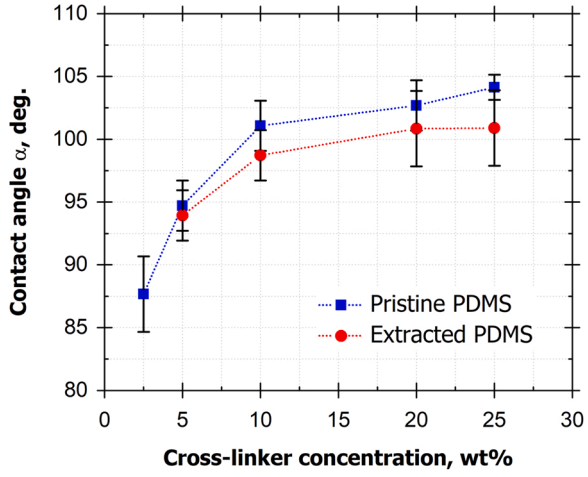

Fig. 1. Water contact angle of pristine (filled square) and extracted (filled circles) PDMS specimens as a function of cross-linker concentration. Error bars represent standard deviation values obtained from 10 measurements at each data point. Lines are only guides for the eye.

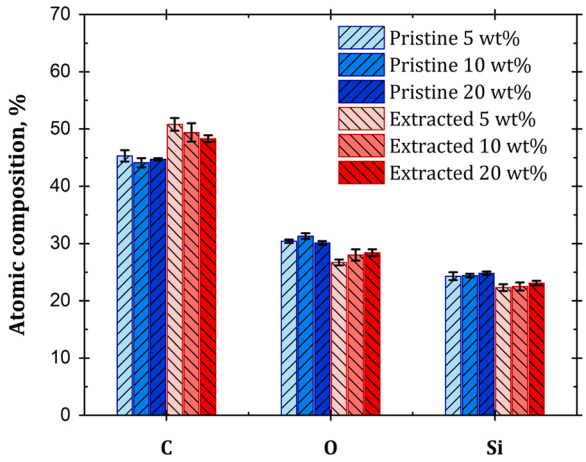

Fig. 2. XPS analysis of pristine and extracted PDMS specimens (atomic compositions for C, O and Si, respectively) as a function of cross-linker concentration. Error bars represent standard deviations of 3 measured values at each data point.

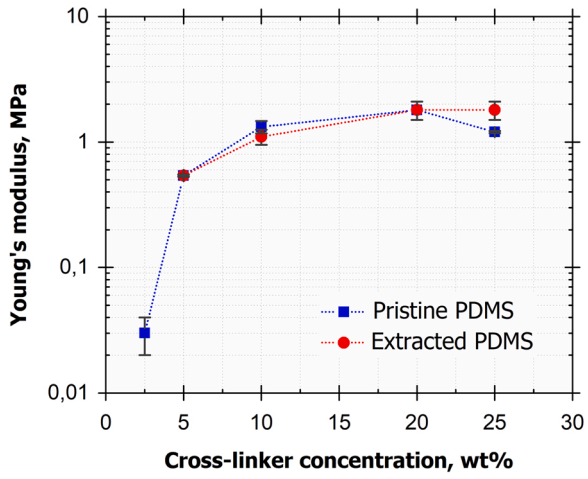

Fig. 3. Bulk Young's modulus of pristine (filled square) and extracted (filled circles) PDMS specimens as a function of cross-linker concentration. Error bars represent SD of 3 measured values at each data point. Lines are only guides for the eye.

$p < 0.05$). However, when the cross-linker concentration was higher than 10 wt%, the Young's modulus value reaches 1.8 MPa and even decreased to 1.2 MPa at 25 wt% cross-linker for the nonextracted PDMS (Student's *t*-test between the modulus values at 20 and 25 wt%, $p < 0.05$).

From the G' and G'' data measured by DMA, it can be seen that the G''/G' ratio at 2.5 wt% increases with frequency tending to 1, which implies high viscous dissipation, whereas at 5 wt% of crosslinker and higher, the viscous component characterized by the loss modulus G'' is essentially negligible (see ESI, Fig. S9). Thus, the PDMS specimens at 5 wt% of crosslinker and higher exhibit a perfectly elastic behavior, whereas the PDMS at 2.5 wt% of crosslinker is still not a percolated network.

The extraction of non-cross-linked free chains from the PDMS network did not noticeably affect the bulk Young's modulus. The Young's moduli of the PDMS samples are listed in Table 1. By comparing the modulus values of the pristine PDMS measured by the standard method at 10 N applied normal force to those measured using in situ curing, one can conclude that the values are similar. Moreover, the Young's modulus values also decrease at higher cross-linker concentrations. Thus, modulus reduction cannot be explained by slip phenomena at the specimen-plate interface that could potentially lead to systematic deviation of the Young's modulus to lower values. A similar reduction of mechanical properties at cross-linker concentrations higher than 10 wt% (balanced stoichiometry between the pre-polymer and the cross-linker) has been reported in earlier studies [30,31]. At the higher cross-linker concentrations cross-link sites are saturated and the excess of cross-linker leads to dilution of the network, thus reducing the modulus. Between 20 and 25 wt% all crosslinking sites are expected to become saturated.

The surface topography can be efficiently imaged by the various modes of AFM. Surface mechanical properties, like dynamic surface modulus, can also be mapped at the nanoscale by Quantitative Dynamic Nanomechanical Analysis (QNM) [32,33]. Regarding the cross-linked PDMS used in this research, we have already reported on surface morphology and stiffness in a detailed QNM study of the PDMS substrates utilized here [34]. For our substrates we first display a larger scan-size height AFM image to capture the rather homogeneous PDMS surfaces. As representative examples, we show in Fig. S10 height scans of PDMS at 5% and 25% crosslinker concentrations, respectively. The surface root mean square roughness, R_{rms}, values were also determined for these and others (larger scan areas) images (for this data see Table S5 in ESI). As one can see, the surface microstructure remains essentially unchanged throughout the crosslink densities employed. The approximately 30% decrease is attributed to the increased stiffness of the specimens with the highest crosslink density.

We then display higher resolution images for each substrate types used in this work, prior to and following extraction (see Fig. 4). The PDMS mesh structure can clearly be seen here. As can be observed on Fig. 4, the network mesh size is only slightly affected by extraction. The average values of the mesh size determined from 200 meshes analyzed for each sample were found to be in the range of 13–16 nm prior to extraction and in the range of 12–13 nm subsequent to extraction (see Table S6). The average R_{rms} values estimated from AFM images taken at five different spots for each sample were found to be in the range of 5–9 nm. Student's *t*-test ($p < 0.001$) revealed a statistically significant decrease in the mesh size subsequent to Soxhlet extraction, except for the specimen at 10 wt% of crosslinker, likely owing to the balanced stoichiometric ratio.

As here we focus on interface adhesion, of high interest are the measurements of the surface Young's moduli values, as obtained by AFM prior, and subsequent, to Soxhlet extraction. As observed in Fig. 5, when increasing the cross-linker concentration to 10 wt%, the surface Young's modulus increases (Student's *t*-test between the modulus values at 5 and 10 wt%, $p < 0.05$). For higher cross-linker concentrations modulus values remain unchanged and even slightly decrease at 25 wt% cross-linker for the nonextracted PDMS (Student's *t*-test between the modulus values at 20 and 25 wt%, $p < 0.05$). While these trends were similar when the surface stiffness dependence was considered, the threshold value was shifted to a significantly higher value of 2.5–2.8 MPa. However, a significant difference, in contrary to what was observed when measuring the storage modulus, is monitored subsequent to Soxhlet extraction. The surface Young's modulus increased following extraction from 0.7 to 2.3 MPa, to 2.1–7.8 MPa. Removal of free PDMS chains by extraction should increase the local crosslink density and thus stiffen the elastomer. On the other hand, elimination of stiff silica would soften the material. We have already shown (see TGA) that extraction removes only very small amounts of silica. As we see a substantial decrease of stiffness with cross-linker concentration (see Fig. 5), we conclude that the trends observed due to Soxhlet treatment are caused by removal of surface-near chains, as extraction increases the surface stiffness. This observation is very relevant as bacteria sense first the surface properties [2], as further evidenced by initial retention studies.

The values of the AFM-measured surface stiffness are however dependent on the bulk crosslink density. During AFM tapping the elastic response of the surface depends on the penetration of the stress field into the material, which depends on the contact force and contact area, and the surface modulus. We reason that during extraction free chains are removed from the surface. This causes local stiffening, which reduces the penetration depth of the stress field. However, enhancement of local stress will result in increasing values of the AFM observed "effective" surface modulus, as pointed out by Sokolov et al. [35].

Fig. 6 shows the number of viable bacteria attached to the surface as a function of the bulk (Fig. 6**a**) and the surface modulus (Fig. 6**b**). Experimentally, the bulk modulus was determined by DMA. We noted that bacterial retention on PDMS samples was inversely proportional to the value of the bulk Young's modulus. This observation is in agreement with the literature [14,36].

Table 1
Comparison between bulk Young's modulus values of pristine and extracted PDMS samples.

Cross-linker concentration [wt%	*Pristine PDMS E [MPa]*	*Extracted PDMS E [MPa]*	*"No-slip" control test E [MPa]*
2.5	**(0.03 ± 0.01)**	***Destroyed***	**(0.06)**
5	**(0.54 ± 0.01)**	**(0.54 ± 0.01)**	**(0.63)**
10	**(1.32 ± 0.15)**	**(1.11 ± 0.15)**	**(1.83)**
20	**(1.8 ± 0.3)**	**(1.8 ± 0.3)**	**(1.68)**
25	**(1.20 ± 0.03)**	**(1.8 ± 0.3)**	**(1.26)**

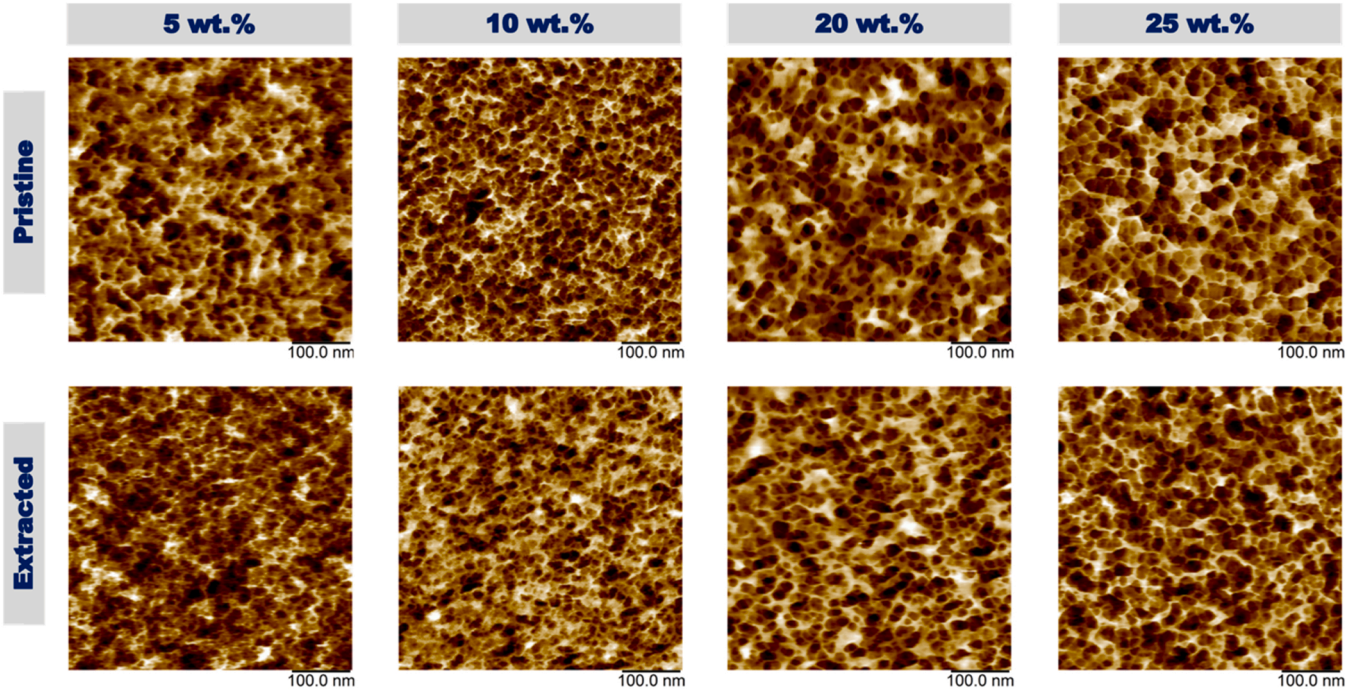

Fig. 4. AFM height images of the free PDMS surfaces prepared at varied cross-linker concentrations prior to (pristine specimen) and subsequent to (extracted specimen) extraction with crosslinker content as indicated. The scan area is 500 nm × 500 nm for all images. The Z-axis ranges from − 30–30 nm.

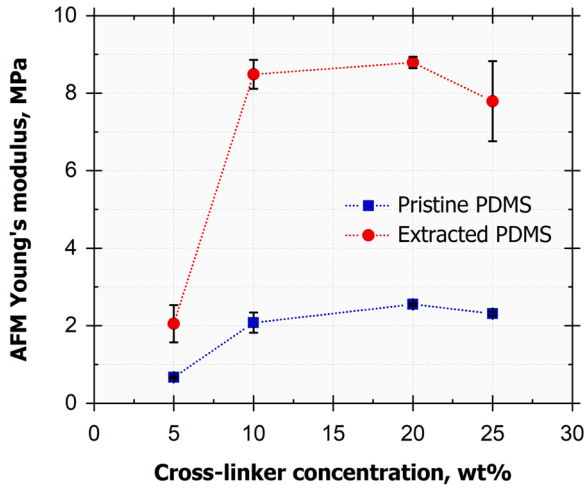

Fig. 5. AFM surface Young's moduli values as function of the crosslinker content (wt%) for pristine and extracted PDMS. (Blue squares: prior to extraction; Red circles: following extraction.). Error bars represent standard deviation values of 3 measurements at each data point. Lines are only guides for the eye.

As shown in Fig. 6a, bacterial retention values on the extracted PDMS samples slightly differ from those on the pristine PDMS specimens. Fig. 6a (data for bulk stiffness) shows that the bacterial retention decreased until a threshold stiffness value at approximately 1.2–1.5 MPa was reached (Pearson correlation analysis, $r = -0.95$, $p < 0.05$). For higher stiffnesses retention remained low, and unchanged. While these trends were similar when the surface stiffness dependence was considered, the threshold value was shifted to a significantly higher value of 2.5–2.8 MPa. Remarkably, this value is essentially the same as the surface modulus of the bacteria. [37,38].

As the bacterial surface Young's modulus is between 2 and 3 MPa [37,38], the outcome of this work suggests that bacterial adhesion of *Escherichia coli* on PDMS is mechanical as hypothesized at first by Song et al. on PDMS of Young's moduli ranging between 0.1 and 2.6 MPa [14]. Compared to earlier work, here we clearly differentiate between surface and bulk moduli of model PDMS. To the best of our knowledge, there is only one study performed by Pan et al. [19] in which the bacterial adhesion was assessed on PDMS substrates as a function of surface stiffness. In this work, Young's modulus of both uncoated PDMS and PDMS coated with a 2 nm highly crosslinked HDMSO was measured using AFM-based nanoindentation to assess near-surface (nm scale) mechanical properties. Interestingly, Young's modulus values were not significantly affected by coating of the PDMS substrates. By contrast, in our investigations the removal of non-crosslinked, free chains causes a substantial increase of surface stiffness. We identify stiffness threshold values above which bacterial retention does not change upon further substrate stiffening. These threshold values differ for the surface and the bulk stiffnesses. The crossover between high and changing bacterial retention and low and constant retention can thus be regarded as a contact mechanics effect between soft surfaces and bacteria. Material stiffness dependence of bacterial retention for Young's modulus values lower than that of the bacterial cell surface is tentatively explained by a conformal overlay between the bacterial and elastomer surfaces, respectively. This effect resembles an elasto-capillary phenomenon, where the interface interaction forces for deformable (or fluid) surfaces are balanced also considering the vertical force component in the Young-Dupre equation (substrate deformation). [39] Due to such elasto-capillary deformations the contact surface between bacteria and substrate are enhanced, as hypothesized earlier by Chen et al. [40]. Above a threshold stiffness this effect is losing its importance. If this overlay becomes essentially inefficient for higher substrate stiffnesses beyond a threshold value, the conformal overlay effect is not any more operational. Essential for retention would thus the combination of the elastic energy of surface deformation and the work of adhesion in the contact area. [41].

4. Conclusions

We investigated initial bacterial retention on model (PDMS) surfaces

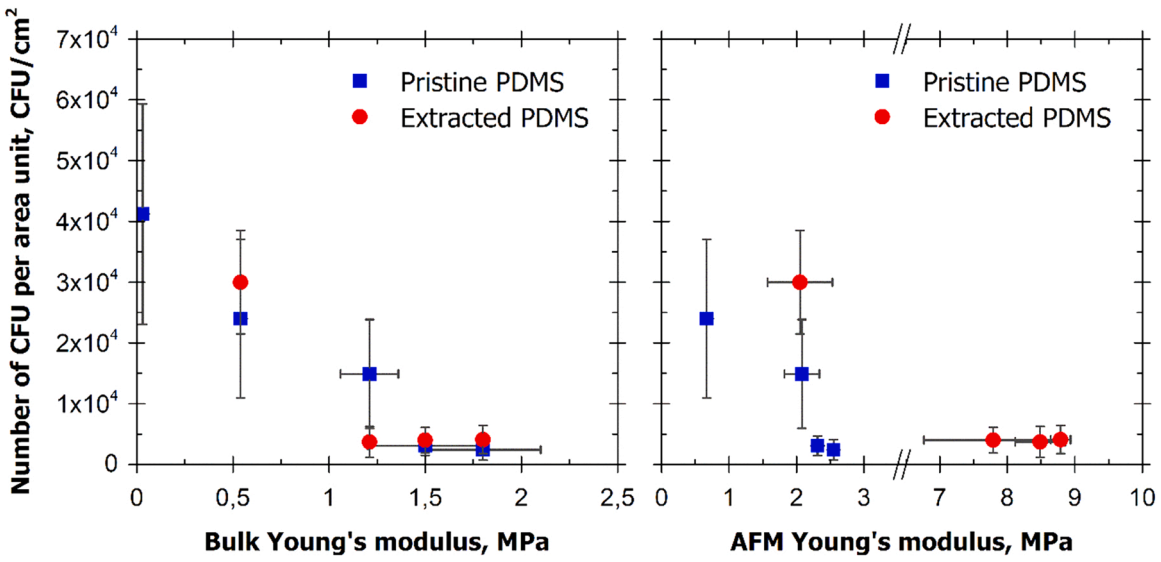

Fig. 6. The number of colony forming units per surface area as a function of a) the bulk Young's modulus (left) and b) the nanoscale (AFM) Young's modulus (right) of the cross-linked PDMS samples. Each data point represents an average of 9 bacterial retention assays performed on 9 different days. Error bars represent standard deviations.

by only varying the mechanical stiffness. Substrates were engineered such that the surface modulus values, as measured by AFM, ranged between 2 and 9 MPa. Following crosslinking, we performed Soxhlet extraction to rule out the effect of non-crosslinked, free chains. The effect of both bulk and surface moduli on bacterial retention were specifically addressed. We combined bulk and advanced surface characterization techniques to demonstrate that neither the surface chemistry nor the surface topography varies with the substrate preparation. We monitored bulk stiffness by DMA and surface stiffness by AFM. The number of bacteria retained, as assessed by initial retention studies, decreases with the increase of both the bulk and the surface mechanical stiffness, and remains essentially unchanged for further stiffening of the substrate beyond a characteristic value that also characterizes bacterial cell wall stiffness. We tentatively explain this observation by considering conformal overlay of bacterial and material surfaces, which might be addressed by considering contact mechanics between bacteria and soft elastomer surfaces.

CRediT authorship contribution statement

Viktoriia Drebezghova: Data collection, analysis, interpretation, drafting the article, critical revision of the article. **Florence Hakil:** data collection, analysis. **Régis Grimaud:** data collection, analysis, interpretation. **Hubert Gojzewski:** data collection, analysis, interpretation. **G. Julius Vancso:** data analysis, interpretation, design of the work, drafting the article, critical revision of the article, final approval of the version to be published. **C. Nardin:** data analysis, interpretation, conception and design of the work, drafting the article, critical revision of the article, final approval of the version to be published.

Declaration of Competing Interest

The authors declare that they have no known competing financial interests or personal relationships that could have appeared to influence the work reported in this paper.

Data Availability

Data will be made available on request.

Acknowledgements

V.D., F.H., R.G. and C.N. thank for funding by the project E2S Université de Pau et des Pays de l'Adour (UPPA, France) (Energy and Environment Solutions) and Programme Interreg V-A Espagne-France-Andorre (POCTEFA) HEALTH LSR 2017–146 (Région Nouvelle Aquitaine, France 1R10103–00013013). H.G. and G.J.V. acknowledge the University of Twente, The Netherlands for financial support. Mr. Gerard Kip and Dr. Yibin Bu (MESA+ Research Institute, Twente) are thanked for their support by XPS analyses.

Appendix A. Supporting information

Supplementary data associated with this article can be found in the online version at doi:10.1016/j.colsurfb.2022.112709.

References

[1] E.P. Magennis, A.L. Hook, M.C. Davies, C. Alexander, P. Williams, M.R. Alexander, Engineering serendipity: high-throughput discovery of materials that resist bacterial attachment, Acta Biomater. 34 (2016) 84–92, https://doi.org/10.1016/j.actbio.2015.11.008.

[2] L. Ploux, A. Ponche, K. Anselme, Bacteria/material interfaces: role of the material and cell wall properties, J. Adhes. Sci. Technol. 24 (13–14) (2010) 2165–2201, https://doi.org/10.1163/016942410×511079.

[3] L. Tallet, V. Gribova, L. Ploux, N.E. Vrana, P. Lavalle, New smart antimicrobial hydrogels, nanomaterials, and coatings: earlier action, more specific, better dosing, Adv. Healthc. Mater. 10 (1) (2021) 2001199, https://doi.org/10.1002/adhm.202001199.

[4] N. Gour, K.X. Ngo, C. Vebert-Nardin, Anti-infectious surfaces achieved by polymer modification: anti-infectious surfaces achieved, Macromol. Mater. Eng. 299 (6) (2014) 648–668, https://doi.org/10.1002/mame.201300285.

[5] R. Wang, B. Zhou, D. Xu, H. Xu, L. Liang, X. Feng, P. Ouyang, B. Chi, Antimicrobial and biocompatible ε-polylysine–γ-poly(Glutamic Acid)–based hydrogel system for wound healing, J. Bioact. Compat. Polym. 31 (3) (2016) 242–259, https://doi.org/10.1177/0883911515610019.

[6] P. Kühn, R. Rozenbaum, E. Perrels, P. Sharma, P. van Rijn, Anti-microbial biopolymer hydrogel scaffolds for stem cell encapsulation, Polymers 9 (12) (2017) 149, https://doi.org/10.3390/polym9040149.

[7] S. Sánchez-Salcedo, M. Colilla, I. Izquierdo-Barba, M. Vallet-Regí, Preventing bacterial adhesion on scaffolds for bone tissue engineering, Int. J. Bioprint. 2 (0) (2016), https://doi.org/10.18063/IJB.2016.01.008.

[8] M.M. Konai, B. Bhattacharjee, S. Ghosh, J. Haldar, Recent progress in polymer research to tackle infections and antimicrobial resistance, Biomacromolecules 19 (6) (2018) 1888–1917, https://doi.org/10.1021/acs.biomac.8b00458.

[9] S. Guo, M.Y. Kwek, Z.Q. Toh, D. Pranantyo, E.-T. Kang, X.J. Loh, X. Zhu, D. Jańczewski, K.G. Neoh, Tailoring polyelectrolyte architecture to promote cell

growth and inhibit bacterial adhesion, ACS Appl. Mater. Interfaces 10 (9) (2018) 7882–7891, https://doi.org/10.1021/acsami.8b00666.
[10] A. Gallardo, E. Martínez-Campos, C. García, A.L. Cortajarena, J. Rodríguez-Hernández, Hydrogels with modulated ionic load for mammalian cell harvesting with reduced bacterial adhesion, Biomacromolecules 18 (5) (2017) 1521–1531, https://doi.org/10.1021/acs.biomac.7b00073.
[11] Q. Cao, S. Wu, L. Wang, X. Shi, G. Li, Effects of the morphology of sulfobetaine zwitterionic layers grafted onto a silicone surface on improving the hydrophilic stability, anti-bacterial adhesion properties, and biocompatibility, J. Appl. Polym. Sci. 135 (44) (2018) 46860, https://doi.org/10.1002/app.46860.
[12] K.W. Kolewe, J. Zhu, N.R. Mako, S.S. Nonnenmann, J.D. Schiffman, Bacterial adhesion is affected by the thickness and stiffness of poly(ethylene glycol) hydrogels, ACS Appl. Mater. Interfaces 10 (3) (2018) 2275–2281, https://doi.org/10.1021/acsami.7b12145.
[13] K.W. Kolewe, S. Kalasin, M. Shave, J.D. Schiffman, M.M. Santore, Mechanical properties and concentrations of poly(ethylene glycol) in hydrogels and brushes direct the surface transport of staphylococcus aureus, ACS Appl. Mater. Interfaces 11 (1) (2019) 320–330, https://doi.org/10.1021/acsami.8b18302.
[14] F. Song, D. Ren, Stiffness of cross-linked Poly(Dimethylsiloxane) affects bacterial adhesion and antibiotic susceptibility of attached cells, Langmuir 30 (34) (2014) 10354–10362, https://doi.org/10.1021/la502029f.
[15] F. Song, M.E. Brasch, H. Wang, J.H. Henderson, K. Sauer, D. Ren, How bacteria respond to material stiffness during attachment: a role of escherichia coli flagellar motility, ACS Appl. Mater. Interfaces 9 (27) (2017) 22176–22184, https://doi.org/10.1021/acsami.7b04757.
[16] F. Song, H. Wang, K. Sauer, D. Ren, Cyclic-Di-GMP and OprF are involved in the response of pseudomonas aeruginosa to substrate material stiffness during attachment on polydimethylsiloxane (PDMS, Front. Microbiol. 9 (2018) 110, https://doi.org/10.3389/fmicb.2018.00110.
[17] S.L. Arias, J. Devorkin, A. Civantos, J.P. Allain, Escherichia coli adhesion and biofilm formation on polydimethylsiloxane are independent of substrate stiffness, Langmuir 37 (1) (2021) 16–25, https://doi.org/10.1021/acs.langmuir.0c00130.
[18] H. Straub, C.M. Bigger, J. Valentin, D. Abt, X.-H. Qin, L. Eberl, K. Maniura-Weber, Q. Ren, Bacterial adhesion on soft materials: passive physicochemical interactions or active bacterial mechanosensing, Adv. Healthc. Mater. 8 (8) (2019) 1801323, https://doi.org/10.1002/adhm.201801323.
[19] F. Pan, S. Altenried, M. Liu, D. Hegemann, E. Bülbül, J. Moeller, W.W. Schmahl, K. Maniura-Weber, Q. Ren, A nanolayer coating on polydimethylsiloxane surfaces enables a mechanistic study of bacterial adhesion influenced by material surface physicochemistry, Mater. Horiz. 7 (1) (2020) 93–103, https://doi.org/10.1039/c9mh01191a.
[20] C.I. Pereni, Q. Zhao, Y. Liu, E. Abel, Surface free energy effect on bacterial retention, Colloids Surf. B: Biointerfaces 48 (2) (2006) 143–147, https://doi.org/10.1016/j.colsurfb.2006.02.004.
[21] D. Hanahan, Studies on transformation of escherichia coli with plasmids, J. Mol. Biol. 166 (4) (1983) 557–580, https://doi.org/10.1016/S0022-2836(83)80284-8.
[22] A. Müller, M.C. Wapler, U. Wallrabe, A quick and accurate method to determine the poisson's ratio and the coefficient of thermal expansion of PDMS, Soft Matter 15 (4) (2019) 779–784, https://doi.org/10.1039/c8sm02105h.
[23] D.K. Owens, R.C. Wendt, Estimation of the surface free energy of polymers, J. Appl. Polym. Sci. 13 (8) (1969) 1741–1747, https://doi.org/10.1002/app.1969.070130815.
[24] J.L. Hutter, J. Bechhoefer, Calibration of atomic-force microscope tips, Rev. Sci. Instrum. 64 (7) (1993) 1868–1873, https://doi.org/10.1063/1.1143970.
[25] Derjaguin, B.V.; Muller, V.M.; Toporov, Y.U.O. Effect of Contact Deformations on the Adhesion of Particles. &çè(, pp 314–326.
[26] S. Josset, N. Keller, M.-C. Lett, M.J. Ledoux, V. Keller, Numeration methods for targeting photoactive materials in the UV-A photocatalytic removal of microorganisms, Chem. Soc. Rev. 37 (4) (2008) 744, https://doi.org/10.1039/b711748p.
[27] Corporation DC (2010/05/03) SYLGARD(R) 184 SILICONE ELASTOMER KIT (BASE). MSDS No: 01064291.
[28] Corporation DC (2011/03/15) SYLGARD(R) 184 SILICONE ELASTOMER KIT (CURING AGENT). MSDS No: 01064291.
[29] E. Delebecq, S. Hamdani-Devarennes, J. Raeke, J.-M. Lopez Cuesta, F. Ganachaud, High residue contents indebted by platinum and silica synergistic action during the pyrolysis of silicone formulations, ACS Appl. Mater. Interfaces 3 (3) (2011) 869–880, https://doi.org/10.1021/am101216y.
[30] A. Mata, A.J. Fleischman, S. Roy, Characterization of polydimethylsiloxane (pdms) properties for biomedical micro/nanosystems, Biomed. Micro 7 (4) (2005) 281–293, https://doi.org/10.1007/s10544-005-6070-2.
[31] J.-H. Seo, K. Sakai, N. Yui, Adsorption state of fibronectin on poly (dimethylsiloxane) surfaces with varied stiffness can dominate adhesion density of fibroblasts, Acta Biomater. 9 (3) (2013) 5493–5501, https://doi.org/10.1016/j.actbio.2012.10.015.
[32] B. Pittenger, S. Osechinskiy, D. Yablon, T. Mueller, Nanoscale DMA with the atomic force microscope: a new method for measuring viscoelastic properties of nanostructured polymer materials, JOM 71 (10) (2019) 3390–3398, https://doi.org/10.1007/s11837-019-03698-z.
[33] R. Garcia, Nanomechanical mapping of soft materials with the atomic force microscope: methods, theory and applications, Chem. Soc. Rev. 49 (16) (2020) 5850–5884, https://doi.org/10.1039/D0CS00318B.
[34] V. Drebezghova, H. Gojzewski, A. Allal, M.A. Hempenius, C. Nardin, G.J. Vancso, Network mesh nanostructures in cross-linked poly(dimethylsiloxane) visualized by AFM, Macromol. Chem. Phys. (2020) 2000170, https://doi.org/10.1002/macp.202000170.
[35] M.E. Dokukin, I. Sokolov, Quantitative mapping of the elastic modulus of soft materials with harmonix and peakforce qnm afm modes, Langmuir 28 (46) (2012) 16060–16071, https://doi.org/10.1021/la302706b.
[36] J.D.P. Valentin, X.-H. Qin, C. Fessele, H. Straub, H.C. van der Mei, M.T. Buhmann, K. Maniura-Weber, Q. Ren, Substrate viscosity plays an important role in bacterial adhesion under fluid flow, J. Colloid Interface Sci. 552 (2019) 247–257, https://doi.org/10.1016/j.jcis.2019.05.043.
[37] A. Cerf, J.-C. Cau, C. Vieu, E. Dague, Nanomechanical properties of dead or alive single-patterned bacteria, Langmuir 25 (10) (2009) 5731–5736, https://doi.org/10.1021/la9004642.
[38] H.H. Tuson, G.K. Auer, L.D. Renner, M. Hasebe, C. Tropini, M. Salick, W.C. Crone, A. Gopinathan, K.C. Huang, D.B. Weibel, Measuring the stiffness of bacterial cells from growth rates in hydrogels of tunable elasticity: measuring cellular mechanical properties with hydrogels, Mol. Microbiol. 84 (5) (2012) 874–891, https://doi.org/10.1111/j.1365-2958.2012.08063.x.
[39] R.W. Style, R. Boltyanskiy, Y. Che, J.S. Wettlaufer, L.A. Wilen, E.R. Dufresne, Universal deformation of soft substrates near a contact line and the direct measurement of solid surface stresses, Phys. Rev. Lett. 110 (6) (2013), 066103, https://doi.org/10.1103/PhysRevLett.110.066103.
[40] Y. Chen, A.K. Harapanahalli, H.J. Busscher, W. Norde, H.C. van der Mei, Nanoscale cell wall deformation impacts long-range bacterial adhesion forces on surfaces, Appl. Environ. Microbiol. 80 (2) (2014) 637–643, https://doi.org/10.1128/AEM.02745-13.
[41] M. Ina, Z. Cao, M. Vatankhah-Varnoosfaderani, M.H. Everhart, W.F.M. Daniel, A. V. Dobrynin, S.S. Sheiko, From adhesion to wetting: contact mechanics at the surfaces of super-soft brush-like elastomers, ACS Macro Lett. 6 (8) (2017) 854–858, https://doi.org/10.1021/acsmacrolett.7b00419.